



1 **Global Spatial Variation in the PM_{2.5} to AOD Relationship Strongly**
2 **Influenced by Aerosol Composition**

3 Haihui Zhu^{1*}, Randall V. Martin¹, Aaron van Donkelaar¹, Melanie S. Hammer¹, Chi Li¹, Jun Meng²,
4 Christopher R. Oxford¹, Xuan Liu¹, Yanshun Li¹, Dandan Zhang¹, Inderjeet Singh¹, Alexei Lyapustin³

5 ¹Department of Energy, Environmental & Chemical Engineering, Washington University in St. Louis, St.
6 Louis, MO, USA

7 ²Department of Civil and Environmental Engineering, Washington State University, Pullman, WA, USA

8 ³Laboratory for Atmospheres, NASA Goddard Space Flight Center, Greenbelt, MD, USA

9 *Correspondence:* Haihui Zhu (haihuizhu@wustl.edu)

10 **Abstract** Ambient fine particulate matter (PM_{2.5}) is the leading global environmental determinant
11 of mortality. However, large gaps exist in ground-based PM_{2.5} monitoring. Satellite remote sensing
12 of aerosol optical depth (AOD) offers information to fill these gaps worldwide, when augmented
13 with a modeled PM_{2.5} to AOD relationship (η). This study aims to understand the spatial pattern
14 and driving factors of η from both observations and modeling. A global observational estimate of
15 η for the year 2019 is inferred from 6,118 ground-based PM_{2.5} measurement sites and satellite
16 retrieved AOD from the MAIAC algorithm. A global chemical transport model, GEOS-Chem, in
17 its high performance configuration (GCHP), is used to interpret the observed spatial pattern of
18 annual mean η . Measurements and the GCHP simulation consistently identify a global population-
19 weighted mean η of 92 – 100 $\mu\text{g}/\text{m}^3$, with regional values ranging from 60.3 $\mu\text{g}/\text{m}^3$ for North
20 America to more than 130 $\mu\text{g}/\text{m}^3$ in Africa. The highest η is found in arid regions where aerosols
21 are less hygroscopic due to mineral dust, followed by regions strongly influenced by surface
22 aerosol sources. Relatively low η is found over regions distant from strong aerosol sources. The
23 spatial variation of η is strongly influenced by aerosol composition driven by its effects on aerosol
24 hygroscopicity. Sensitivity tests with globally uniform parameters reveal that aerosol composition
25 leads to the strongest η spatial variability, with a population-weighted normalized mean difference
26 of 12.3 $\mu\text{g}/\text{m}^3$, higher than that from aerosol vertical profile (8.4 $\mu\text{g}/\text{m}^3$), reflecting the determinant
27 composition effects on aerosol hygroscopicity and aerosol optical properties.



28 **1 Introduction**

29 Exposure to ambient fine particulate matter ($PM_{2.5}$) has been recognized as the predominant
30 environmental risk factor for the global burden of disease, leading to millions of deaths annually
31 (Murray et al., 2020; Burnett et al., 2018). Even at low $PM_{2.5}$ concentrations, long-term exposure
32 can increase circulatory and respiratory related mortality (Pinault et al., 2016; Christidis et al.,
33 2019; Weichenthal et al., 2022). Despite the importance of $PM_{2.5}$, many of the world's countries
34 do not provide publicly accessible $PM_{2.5}$ data (Martin et al., 2019). Satellite remote sensing of
35 aerosol optical depth (AOD), an optical measure of aerosol abundance, offers information about
36 the distribution of $PM_{2.5}$ (Kondragunta et al., 2022). A large community relies upon the spatial
37 distribution of $PM_{2.5}$ concentrations inferred from satellite remote sensing for health impact
38 assessment and epidemiological analyses of long-term exposure (Murray et al., 2020; Burnett et
39 al., 2018; Hao et al., 2023; Cohen et al., 2017). Quantitative application of satellite AOD for long-
40 term characterization of the spatial distribution of $PM_{2.5}$ would benefit from a better understanding
41 of the factors affecting the $PM_{2.5}$ -AOD relationship.

42 The relationship between satellite AOD and surface $PM_{2.5}$ can be established through a statistical
43 method, a geophysical method, or their combination. A statistical method uses ground-based
44 monitors for training and is well suited for regions with dense monitors (Xin et al., 2014; Hu et al.,
45 2014; Di et al., 2016). A geophysical approach utilizes a chemical transport model to simulate the
46 relationship (η) between $PM_{2.5}$ and AOD for application to satellite AOD (van Donkelaar et al.,
47 2006, 2010; He et al., 2021), and thus depends on accurate model representation of η . van
48 Donkelaar et al. (2015, 2016) combined the two methods by applying geographically weighted
49 regression (GWR) on the geophysical $PM_{2.5}$, which further constrains geophysical $PM_{2.5}$ using
50 ground measurements and other predictors. However, accuracy of geophysical $PM_{2.5}$ remains
51 critical over vast areas with sparse monitoring, and knowledge about the factors affecting η spatial
52 variability are needed to guide improvements of modeled η and geophysical $PM_{2.5}$.

53 Previous studies have identified several factors that affect η variability, including aerosol vertical
54 distribution, aerosol hygroscopicity, aerosol optical properties, and ambient meteorological factors
55 such as relative humidity (RH), planetary boundary layer height (PBLH), wind speed, temperature,
56 and fire events (Wendt et al., 2023; Jin et al., 2019; Guo et al., 2017; Ford and Heald, 2015; Li et
57 al., 2015; van Donkelaar et al., 2013). Most studies focused on the temporal variability of η and



58 found association with meteorological variables such as PBLH (Yang et al., 2019; He et al., 2021;
59 Chu et al., 2015; Gupta et al., 2006; Zhang et al., 2009; Damascena et al., 2021). A few studies
60 have examined the regional-scale spatial variation of η with meteorological, land type variables,
61 and aerosol vertical profile in North America (Jin et al., 2020; van Donkelaar et al., 2006; Li et al.,
62 2015) and China (Yang et al., 2019). To our knowledge, none have examined the factors at the
63 global scale affecting the spatial variation of η or the effects of chemical composition.

64 In this work, we examine this knowledge gap about the spatial variation in η at a global scale. We
65 first collect data from more than 6,000 $\text{PM}_{2.5}$ monitoring sites provided by nine networks and
66 satellite AOD to obtain an observationally based map of η . We further interpret the global η using
67 the GEOS-Chem model of atmospheric composition with recent improvements in aerosol size
68 representation, $\text{PM}_{2.5}$ diel variation, and vertical allocation. By decomposing the simulated η , we
69 identify 2 strong drivers of η spatial variability: aerosol composition and aerosol vertical profile.
70 We conduct sensitivity tests using GEOS-Chem to study how the two factors vary globally and
71 how they contribute to the spatial variation in η .

72 **2 Methods**

73 **2.1 Ground Measured $\text{PM}_{2.5}$**

74 We collect ground-based measurements of $\text{PM}_{2.5}$ for the year 2019 from which to produce
75 observational constraints on η . We obtain $\text{PM}_{2.5}$ measurements from 7 regional networks and 2
76 global networks, as shown in Figure A1. For the United States, we access data from the United
77 States Environmental Protection Agency's Air Quality System (<https://www.epa.gov/outdoor-air-quality-data/download-daily-data>), including both Federal Reference Method and non-Federal
78 Reference Methods $\text{PM}_{2.5}$ (e.g. IMPROVE network). $\text{PM}_{2.5}$ data for Canada are from the
79 Environment Canada's National Air Pollution Surveillance (NAPS) program. $\text{PM}_{2.5}$ data for
80 Europe are from the European Environment Agency Air Quality e-Reporting system
81 (<https://www.eea.europa.eu/data-and-maps/data/aqereporting>). Over mainland China, $\text{PM}_{2.5}$
82 measurements are downloaded from <http://beijingair.sinaapp.com/>, which provides instantaneous
83 air quality data records from the National and Provincial Environmental Protection Agencies. Over
84 India, $\text{PM}_{2.5}$ data are originally from the Central Pollution Control Board Continuous Ambient Air
85 Quality Monitoring network and the U.S. embassies. Over Australia, observations are downloaded
86



87 for the Northern Territory (<http://ntepa.webhop.net/NTEPA/>), Queensland
88 (<https://www.data.qld.gov.au/dataset/>), and New South Wales ([https://www.dpie.nsw.gov.au/air-](https://www.dpie.nsw.gov.au/air-quality/air-quality-data-services/data-download-facility)
89 [quality/air-quality-data-services/data-download-facility](https://www.dpie.nsw.gov.au/air-quality/air-quality-data-services/data-download-facility)). We require at least 5 days of
90 measurements for each month for a monitor to be included. Additionally, we obtain PM_{2.5}
91 measurements over other regions provided by the World Health Organization (WHO) Global
92 Ambient Air Quality Database and by the Surface PARTiculate mAtter Network Network
93 (SPARTAN), which is co-located with the Aerosol Robotic Network (AERONET). SPARTAN
94 also provides filter based PM_{2.5} chemical composition, which is initially described in Snider et al.,
95 (2016). Subsequent developments to the sampling and analysis procedure of SPARTAN include
96 an upgrade to the AirPhoton SS5 sampling station to use a cyclone inlet, an automated weighing
97 system (MTL AH500E) to improve precision and throughput, additional black carbon analysis by
98 Hybrid Integrating Plate/Sphere (White et al., 2016), trace metal elements measured by X-ray
99 Fluorescence (Liu et al., 2024) and a global mineral dust equation (Liu et al., 2022). We require
100 50 days of coincident PM_{2.5} and AERONET AOD measurements for a SPARTAN site to be
101 included in our analysis.

102 **2.2 Satellite AOD**

103 We obtain AOD at 550 nm from the Multi-Angle Implementation of Atmospheric Correction
104 (MAIAC) algorithm, which offers AOD at a high spatial resolution of 1 km worldwide over both
105 land and coastal regions (Lyapustin et al., 2018). The radiances used in the retrieval are measured
106 by the twin MODerate resolution Imaging Spectroradiometer (MODIS) instruments onboard the
107 Terra and Aqua satellites. Terra follows a descending orbital path, crossing the equator at 10:30
108 local time, while Aqua is on an ascending orbit with 13:30 equatorial crossing local time. Both
109 MODIS instruments offer a wide swath width of 2330 km, enabling nearly global daily coverage
110 of the Earth (Sayer et al., 2014). PM_{2.5} monitoring sites with annual mean satellite AOD less than
111 0.05 (background AOD level over land) are excluded to reduce the influence of retrieval
112 uncertainties on our analysis.

113 **2.3 AERONET AOD**

114 AERONET is a worldwide sun photometer network that provides long-term measurement of AOD.
115 We use the Version 3 Level 2 database, which includes an improved cloud screening algorithm



116 (Giles et al., 2019). We sample AERONET AOD within ± 15 min of the satellite overpass time and
117 interpolate to 550 nm wavelength, based on the local Ångström exponent at 440 and 670 nm. For
118 SPARTAN sites, we sample AERONET data coincidentally with SPARTAN aerosol composition
119 to obtain the ground-based observation of η .

120 **2.4 GEOS-Chem Simulation**

121 We simulate η with the GEOS-Chem chemical transport model (www.geos-chem.org, last access:
122 26 October 2023), driven by offline meteorological data, MERRA-2, from the Goddard Earth
123 Observing System (GEOS) of the NASA Global Modeling and Assimilation Office (Schubert et
124 al., 1993). We use the high-performance configuration of GEOS-Chem (GCHP) (Eastham et al.,
125 2018) version 13.4.0 (DOI: 10.5281/zenodo.7254268), which includes advances in performance
126 and usability (Martin et al., 2022). The simulation is conducted for the year 2019, on a C90 cubed-
127 sphere grid corresponding to a horizontal resolution of about 100 km, with a spin-up time of 1
128 month.

129 The GEOS-Chem aerosol simulation includes the sulfate-nitrate-ammonium (SNA) system
130 (Fountoukis and Nenes, 2007), primary and secondary carbonaceous aerosols (Park et al., 2003;
131 Wang et al., 2014; Pai et al., 2020), sea salt (Jaeglé et al., 2011), and natural (Fairlie et al., 2007;
132 Meng et al., 2021) and anthropogenic (Philip et al., 2017) dust. The primary emission data are
133 from the Community Emissions Data System (CEDS_{GBD-MAPS}; McDuffie et al., 2020). Emissions
134 from stacks are distributed vertically (Bieser et al., 2011). Diel variation of anthropogenic
135 emissions is included (Li et al., 2023). Resolution-dependent soil NO_x, sea salt, biogenic VOC,
136 and natural dust emissions are calculated offline at native meteorological resolution to produce
137 consistent emissions across resolutions (Weng et al., 2020; Meng et al., 2021). Biomass burning
138 emissions use the Global Fire Emissions Database, version 4 (GFED4) at daily resolution (van der
139 Werf et al., 2017). We estimate organic matter (OM) from primary organic carbon using an
140 OM/OC parameterization (Philip et al., 2014; Canagaratna et al., 2015). For secondary aerosol
141 components, the concentration at 2 m above the surface is used to calculate PM_{2.5}, following Li et
142 al. (2023). A 50% reduction of the surface nitrate concentration is applied to account for the long-
143 persisting bias in surface nitrate simulated by GEOS-Chem (Heald et al., 2012; Zhang et al., 2012;
144 Zhai et al., 2021; Miao et al., 2020; Travis et al., 2022) and other models (Zakoura and Pandis,



145 2018; Shimadera et al., 2014). Dry and wet deposition follows Amos et al. (2012), with a standard
146 resistance-in-series dry deposition scheme (Wang et al., 1998). Wet deposition includes
147 scavenging processes from convection and large-scale precipitation (Liu et al., 2001).

148 Global RH-dependent aerosol optical properties are based on the Global Aerosol Data Set (GADS)
149 (Kopke P., 1997), as originally implemented by Martin et al. (2003), with updates for SNA and
150 OM dry size (Zhu et al., 2023), hygroscopicity (Latimer and Martin, 2019), mineral dust size
151 distribution (Zhang et al., 2013), and absorbing brown carbon (Hammer et al., 2016). We
152 artificially increase simulated AOD by 0.04 globally to address a poorly understood systematic
153 bias. PM_{2.5} is calculated as the sum of each component at 35% RH to align with common
154 measurement protocols.

155 **2.5 Population**

156 Global population information is obtained from the Gridded Population of the World provided by
157 the NASA Socioeconomic Data and Applications Center (Center for International Earth Science
158 Information Network - CIESIN - Columbia University, 2018).

159 **2.6 Sensitivity Tests with Globally Uniform Parameters**

160 We conduct sensitivity tests of factors affecting the spatial variation of η , with a focus on aerosol
161 composition and aerosol vertical profile. To understand the relative importance of these factors,
162 we impose a constant for each factor and simulate the corresponding η . The difference between
163 the test scenario and the base scenario reflects the change due to variation of the factor. We use
164 the global population-weighted mean (PWM) and population-weighted mean difference (PWMD)
165 to summarize changes with a focus on relevance to population exposure:

$$X_{PWM} = \frac{\sum_j \sum_i P_{i,j} X_{i,j}}{\sum_j \sum_i P_{i,j}}$$

166

$$PWMD = \frac{\sum_j \sum_i P_{i,j} |X_{i,j} - Y_{i,j}|}{\sum_j \sum_i P_{i,j}}$$

167 where i and j are grid box identifiers. X and Y could be any variable of interest. $|X_{i,j} - Y_{i,j}|$ is the
168 absolute value of their difference.



169 The first test imposes globally uniform aerosol chemical composition calculated as the global
170 PWM aerosol component fraction ($F_{s,k,PWM}$):

$$F_{s,k,PWM} = \frac{\sum_j \sum_i P_{i,j} F_{i,j,s,k}}{\sum_j \sum_i P_{i,j}}$$

171 where i , j , and k are grid box identifiers along latitude, longitude, and vertical layer. P represents
172 population density in each grid box. F_s is the fraction of aerosol component S in total aerosol mass.
173 This test keeps the total columnar aerosol mass and aerosol vertical profile unchanged.

174 The second test imposes a globally uniform aerosol vertical profile calculated as the PWM column
175 relative vertical profile ($R_{s,k,PWM}$):

$$R_{s,k,PWM} = \frac{\sum_j \sum_i P_{i,j} R_{i,j,k,s}}{\sum_j \sum_i P_{i,j}}$$

176 where $R_{i,j,k,s}$ is the relative dry mass ratio compared to the surface. The total mass loading and
177 relative chemical composition are unchanged.

178 We analyze global and regional variations of η , as well as that for the driving factors. The definition
179 of each region used in this study is summarized in Figure A2.

180 **3 Results and Discussion**

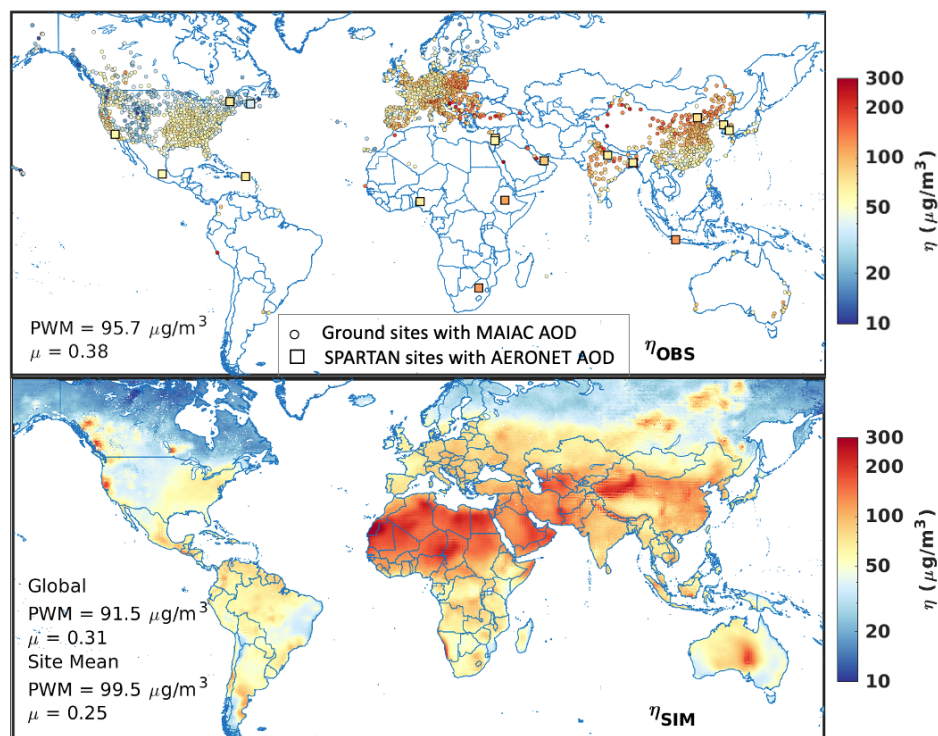
181 **3.1 Global Spatial Pattern of η**

182 The top panel of Figure 1 shows the observationally based annual mean η , inferred from the ratio
183 of ground-measured $PM_{2.5}$ to MAIAC AOD. Measurements are most dense in North America,
184 Europe, and East Asia. The annual mean η varies substantially, from $7.8 \mu\text{g}/\text{m}^3$ in Hawaii to 321
185 $\mu\text{g}/\text{m}^3$ in Central Asia, with a PWM of $95.7 \mu\text{g}/\text{m}^3$ and standard deviation (σ) of $36.6 \mu\text{g}/\text{m}^3$. Higher
186 PWM η of $132 \mu\text{g}/\text{m}^3$ to $154 \mu\text{g}/\text{m}^3$ exist over desert regions such as the North Africa and West
187 Asia, followed by PWM η of $97 \mu\text{g}/\text{m}^3$ to $121 \mu\text{g}/\text{m}^3$ by regions strongly influenced by
188 anthropogenic aerosols, such as East Asia, South Asia (Figure A3 and Table A1). Over North
189 America, η is around $60 \mu\text{g}/\text{m}^3$ in the east and in California, which is more than double that in the
190 Rockies, driven by the spatial pattern of surface $PM_{2.5}$ (Figure A3). The PWM η in North America
191 of $60.3 \mu\text{g}/\text{m}^3$ is about 30% lower than the global PWM. The η pattern found here is similar to that
192 reported by Jin et al. (2020) for the U.S. In Europe, η also varies noticeably between the east and



193 the west, driven by the spatial pattern of surface $PM_{2.5}$, as $PM_{2.5}$ increases by 60% from west to
194 east while AOD increases by only 8%. The PWM η in Europe is $94.0 \mu\text{g}/\text{m}^3$, slightly lower than
195 the global PWM. In Asia, measured η is concentrated in China and India. In China, the η spatial
196 pattern shows a clear distinction between the northern and southern regions, driven by the higher
197 AOD in the south, where relative humidity is high. A similar η spatial pattern and a negative
198 correlation between η and RH are reported by Yang et al. (2019). In India, η is highest in the
199 northwest, with a PWM η of $128 \mu\text{g}/\text{m}^3$, and decreases to about $80 \mu\text{g}/\text{m}^3$ toward the east and the
200 south. Both $PM_{2.5}$ and AOD follow the same spatial pattern, while $PM_{2.5}$ exhibits a stronger
201 decreasing tendency. PWM η in Asia is $100 \mu\text{g}/\text{m}^3$, the highest among the populous regions and
202 4.5% higher than the global PWM. Globally, from west to east, η increases by about 62%, despite
203 that both $PM_{2.5}$ and AOD increased more than threefold (Figure A5). The coefficient of variation
204 (standard deviation divided by mean) in η is higher in Europe ($\mu = 0.31$) and Asia ($\mu = 0.34$), than
205 North America ($\mu = 0.23$, Figure A5).

206 The bottom panel in Figure 1 shows the GCHP simulated η , the ratio between simulated 24-hour
207 mean surface $PM_{2.5}$ and simulated total column AOD at satellite overpass time. The simulation
208 generally reproduces the global observations of η with a tendency for high values in arid regions
209 influenced by dust and low values in regions distant from strong surface sources. The global
210 simulated PWM η is 4% higher than the observations ($99.5 \mu\text{g}/\text{m}^3$ vs. $95.7 \mu\text{g}/\text{m}^3$), mostly driven
211 by an overestimation in Asia ($107 \mu\text{g}/\text{m}^3$ vs. $100 \mu\text{g}/\text{m}^3$), that reflects an overestimation of PWM
212 $PM_{2.5}$ ($47.0 \mu\text{g}/\text{m}^3$ vs. $43.6 \mu\text{g}/\text{m}^3$). The simulation generally reproduces the regional spatial pattern
213 in North America and Asia but underestimates the η variability in Europe as it overestimates η in
214 central Europe and underestimates η in Eastern Europe, due to positive bias in simulated $PM_{2.5}$ in
215 central Europe and positive bias in simulated AOD in Eastern Europe. Nonetheless, the PWM η
216 in Europe ($84.1 \mu\text{g}/\text{m}^3$) is within 11% of observations. Globally, there is overall consistency
217 between the simulated η and observed η , with a correlation of 0.64, resulting in a high degree of
218 consistency between geophysical $PM_{2.5}$ and measured $PM_{2.5}$ ($r = 0.90$, Figure A5).



219

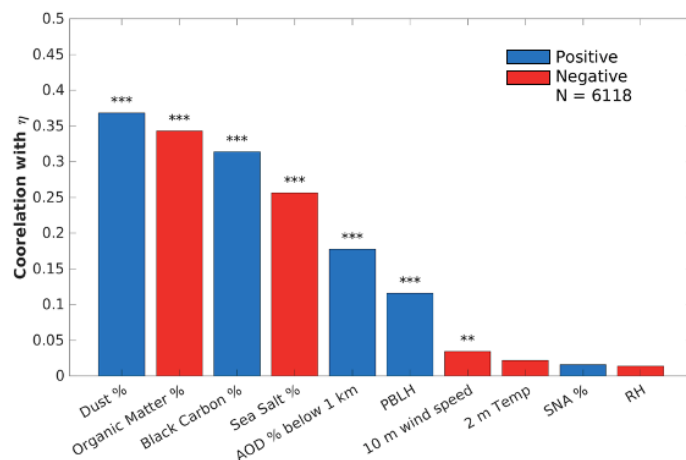
220 Figure 1. Observed (top) and simulated (bottom) annual mean η for 2019. Circles represent ground
 221 measurement sites from regional networks or the World Health Organization. Squares represent co-
 222 located ground measured $\text{PM}_{2.5}$ from SPARTAN and AOD from AERONET. PWM = population-
 223 weighted mean, μ = coefficient of variation (standard deviation divided by mean).

224 We explore the dominant driving factors for η spatial variation by calculating the spatial
 225 correlation between each candidate factor and the observation-based η . Candidate factors
 226 examined include meteorological fields (MERRA-2), aerosol vertical profile, and aerosol
 227 composition as collected from the GCHP simulation or SPARTAN. Meteorological fields include
 228 those commonly considered to represent the temporal variation in η , such as PBLH, RH at 700
 229 hPa, wind speed at 10 m, and temperature at 2 m (Yang et al., 2019; He et al., 2021; Chu et al.,
 230 2015; Damascena et al., 2021). The aerosol vertical profile is represented as the AOD fraction
 231 below 1 km (AOD % below 1 km). Aerosol composition includes SNA, OM, dust, black carbon,
 232 and sea salt, all represented as the fractional contributions (%) to surface $\text{PM}_{2.5}$. Figure 2 shows
 233 the spatial correlation of annual mean factors versus observation-based η . Aerosol components,



234 particularly those with strong primary sources (dust, OM, and black carbon), exhibit the strongest
235 correlations (>0.3) with observationally based η . Significant positive correlations are found for
236 mineral dust and black carbon, both of which are non- or weakly-hygroscopic. Significant negative
237 correlations are found for organic matter and sea salt, reflecting a weak connection between surface
238 concentrations and AOD aloft. Processes are further discussed in sections 3.2 and 3.4. The aerosol
239 vertical profile exhibits a moderate correlation with η (0.18), which is notably higher than any
240 meteorological factors (<0.12). Ground-based data from SPARTAN and AERONET corroborate
241 the correlation between aerosol composition and η (Figure A6).

242 The indicators of spatial variation in η found here differ from that for temporal variation of η in
243 prior work (e.g. He et al. 2021), reflecting the different processes involved. Meteorological
244 parameters drive short-term variability in the aerosol vertical profile, such as day-to-day variation
245 in mixed layer depth or in advection from a point source. In contrast, the spatial variation in annual
246 mean η reflects the spatial variation in processes affecting the long-term relation of surface $\text{PM}_{2.5}$
247 at controlled RH of 35% with AOD at ambient RH. Aerosol composition and the aerosol vertical
248 profile reflect spatial variation in aerosol hygroscopicity, mass extinction efficiency, and sources.
249 The following sections explore how aerosol composition and aerosol vertical profile vary globally
250 and examine how they affect the spatial pattern of η by conducting two sensitivity tests. In each
251 sensitivity test, we replace the spatial variability of a factor with a globally uniform value. The
252 variability of aerosol composition and aerosol vertical profile are discussed in sections 3.2 and 3.3,
253 respectively. The sensitivity test results are discussed in section 3.4.



254

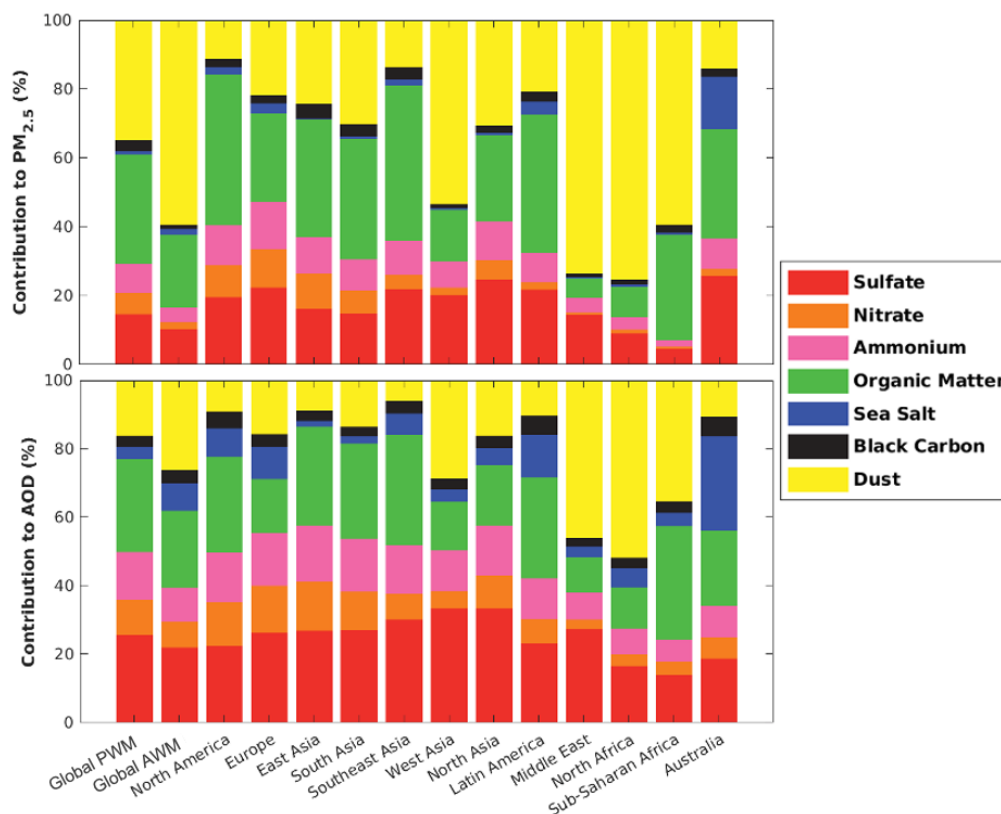
255 Figure 2. Spatial correlation between annual mean modeled parameters and observationally-based η . Blue
 256 bars indicate positive correlations. Red bars indicate negative correlations. Stars above each bar indicate
 257 the p-value associated with each correlation. ‘***’ indicates the p-value is lower than 0.001 and ‘**’
 258 indicates lower than 0.01.

259 3.2 Spatial Variability in Aerosol Composition

260 Figure 3 shows the simulated PWM aerosol composition globally and regionally, as well as the
 261 global area-weighted mean (AWM). The top panel shows the compositional contribution to $PM_{2.5}$.
 262 Globally, dust is the leading PWM $PM_{2.5}$ component (34.7%), followed by OM (31.9%) and SNA
 263 (29.3%). The bottom panel shows the compositional contribution to AOD. PWM AOD
 264 composition is more evenly distributed, with more contribution from SNA (49.9%), followed by
 265 OM (27.2%) and dust (16.1%). Overall, more hygroscopic aerosols such as SNA tend to contribute
 266 a larger fraction of AOD which is at ambient RH, while less hygroscopic aerosols, such as mineral
 267 dust tend to contribute a larger fraction of $PM_{2.5}$ which is at controlled RH of 35%. The AWM
 268 $PM_{2.5}$ and AOD composition exhibit weaker contributions from SNA, primarily reflecting a larger
 269 contribution from dust in remote regions than in more densely populated areas. Over populous
 270 regions such as North America, Europe, and Southeast Asia, there are greater SNA and OM
 271 fractions than the global mean (Figure 3). Arid regions, such as West Asia, the Middle East, North
 272 Africa, and Sub-Saharan Africa, have large fractions of non-hygroscopic mineral dust that (1)
 273 reduce aerosol mass extinction efficiency, yielding less AOD per unit mass, and (2) are unaffected



274 by the controlled RH of $PM_{2.5}$. Both of these factors increase η in dusty regions compared with
 275 regions dominated by hygroscopic SNA aerosols.



276

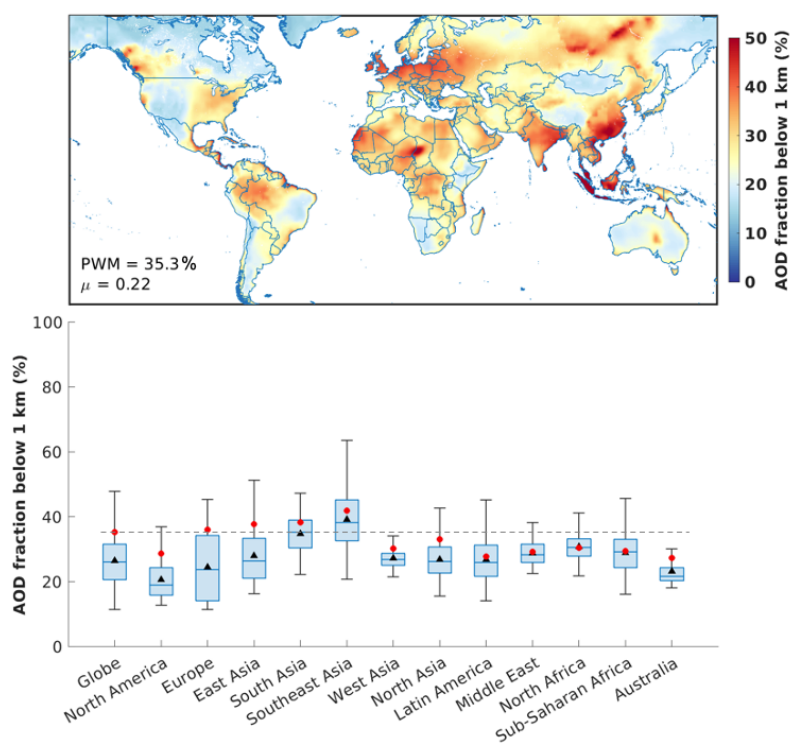
277 Figure 3. Global and regional PWM contributions of aerosol composition to surface $PM_{2.5}$ (top) and AOD
 278 (bottom). The global area-weighted mean (AWM) over land is also included as the second column.

279 3.3 Spatial Variability in Aerosol Vertical Profile

280 Figure 4 shows the AOD fraction below 1 km in the GEOS-Chem simulation. Globally, 35.3% of
 281 the PWM AOD is below 1 km. The PWM value is greater than the AWM value since populated
 282 areas tend to have more surface emissions of particles and precursors. Over North America, Europe,
 283 and East Asia, the PWM surface AOD fractions are much higher than the medians and AWM,
 284 indicating high spatial heterogeneity between urban and remote areas. Europe exhibits the highest
 285 variation and the largest discrepancy between PWM and AWM, reflecting the largest spatial
 286 heterogeneity in aerosol vertical profile, driven by influences from regional pollution, marine



287 aerosols, and transported dust (Zhao et al., 2018). Southeast Asia has the highest surface AOD
 288 fraction and a large variation. Local sources, long-range transported dust, and the influence of
 289 trade winds all contribute to the unique spatial variation in aerosol vertical profile in this region
 290 (Nguyen et al., 2019; Banerjee et al., 2021). Globally, PWM values exhibit less variation than
 291 AWM, indicating moderate variation in aerosol profile across populous areas.



292

293 Figure 4. (Top) Map of AOD fraction below 1 km. (Bottom) Global and regional statistics for AOD
 294 fraction below 1 km. Black triangles show the area-weighted mean. Red circles show the PWM. The line
 295 inside each box is the sample median. Each box's top and bottom edges are the 75 and 25 quartiles,
 296 respectively. Vertical bars are the maximum and minimum values within 1.5 times the interquartile range.
 297 The dashed line indicates global PWM.

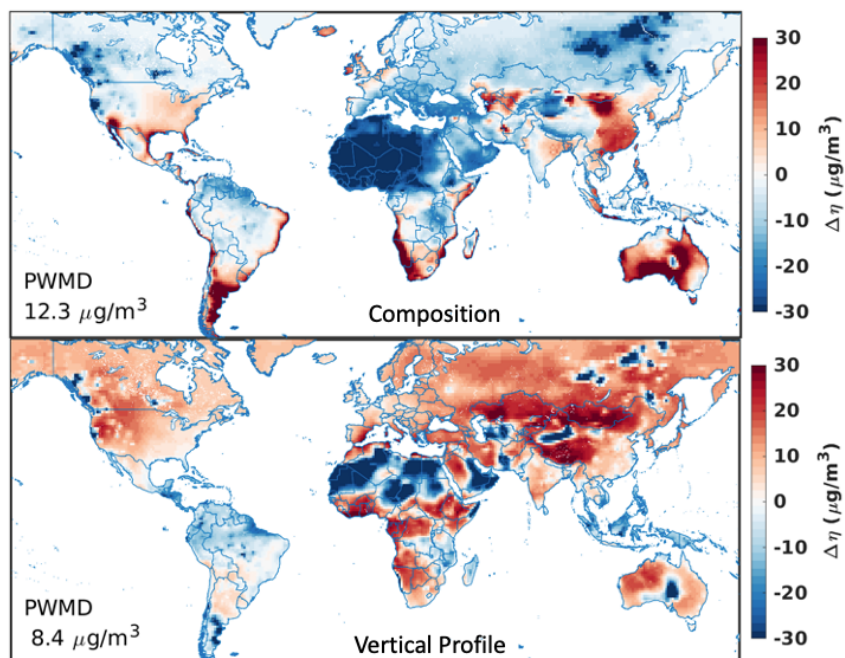
298 3.4 Sensitivity Tests with Globally Uniform Parameters

299 Figure 5 shows the global changes in the spatial variation in η due to variations in aerosol chemical
 300 composition (top) and aerosol vertical profile (bottom). Globally, neglect of spatial variation in



301 aerosol composition induces a $12.3 \mu\text{g}/\text{m}^3$ PWMD in η spatial variation. Both $\text{PM}_{2.5}$ and AOD are
302 strongly affected by aerosol composition, following a similar spatial pattern (Figure A7). Over
303 mid- and low-latitude areas, the change in AOD is stronger than in $\text{PM}_{2.5}$, which gives the opposite
304 pattern in the η . Neglect of spatial variation in chemical composition reduces η over North Africa
305 and the Middle East, desert regions where aerosols contain more weakly hygroscopic components
306 such as mineral dust, compared to populous areas, which contain more secondary inorganic aerosol
307 (Figure 3). For smaller deserts in the Southwest U.S., Argentina, and Southwest Africa, the dust
308 fractions of surface aerosols are higher than the global mean (36%, 76%, and 49%, respectively),
309 but the dust fraction for AOD is similar to the global mean (15%, 25%, and 14%, respectively).
310 Therefore, neglect of the spatial variation of chemical composition increases η over these small
311 deserts by increasing the fraction of hygroscopic components in $\text{PM}_{2.5}$ and leaving AOD almost
312 unchanged (Figure A7). It also reduces η over the boreal forests and the Amazon, where surface
313 aerosols contain little dust and are more hygroscopic compared to populous areas (Figure 3).
314 Neglect of spatial variation in chemical composition increases η over the eastern U.S. and eastern
315 China, where $\text{PM}_{2.5}$ contains more hygroscopic SNA and less dust than the global mean. It also
316 increases η in coastal regions where aerosol contains more hygroscopic sea salt than the global
317 mean.

318 Neglect of spatial variation in the aerosol vertical profile induces an $8.4 \mu\text{g}/\text{m}^3$ PWMD in η spatial
319 variation (Figure 5), following the spatial pattern of the change in surface $\text{PM}_{2.5}$ (Figure A8). The
320 most apparent feature is an increase in η throughout the remote northern hemisphere, driven by an
321 increased aerosol fraction near the surface where the fraction is normally small (Figure 4). The
322 uniform aerosol vertical profile decreases η over northern Africa and biomass burning regions of
323 the boreal forests, the Amazon, and Indonesia, driven by a decreased aerosol fraction near the
324 surface in regions where that fraction is normally high.



325

326 Figure 5. Changes in η (test -base) for each sensitivity test. In the first test, a global PWM aerosol
327 composition replaces the actual composition (top). In the second test, a global PWM aerosol profile
328 replaces the actual profiles (bottom). Numbers inset indicate population-weighted mean difference
329 (PWMD).

330 Conclusion

331 Understanding the global variation of the $PM_{2.5}$ and AOD relationship (η) offers insight into the
332 geophysical inference of $PM_{2.5}$ from satellite AOD observations. We collected ground-based $PM_{2.5}$
333 measurements from 6188 sites and MODIS MAIAC satellite AOD throughout the year 2019 to
334 obtain, for the first time, a global scale observationally based η map. Observed annual mean η
335 ranges from $7.8 \mu\text{g}/\text{m}^3$ in Hawaii to $321 \mu\text{g}/\text{m}^3$ in Central Asia. We observed enhanced η of 132
336 $\mu\text{g}/\text{m}^3$ to $154 \mu\text{g}/\text{m}^3$ over arid regions such as North Africa and West Asia, due to their low aerosol
337 extinction efficiency. Moderate η of $97 \mu\text{g}/\text{m}^3$ to $121 \mu\text{g}/\text{m}^3$ was found in industrial areas such as
338 East Asia and South Asia, where anthropogenic emissions increase the near-surface $PM_{2.5}$
339 concentrations. Over remote areas, low η ($< 50 \mu\text{g}/\text{m}^3$) was usually observed.



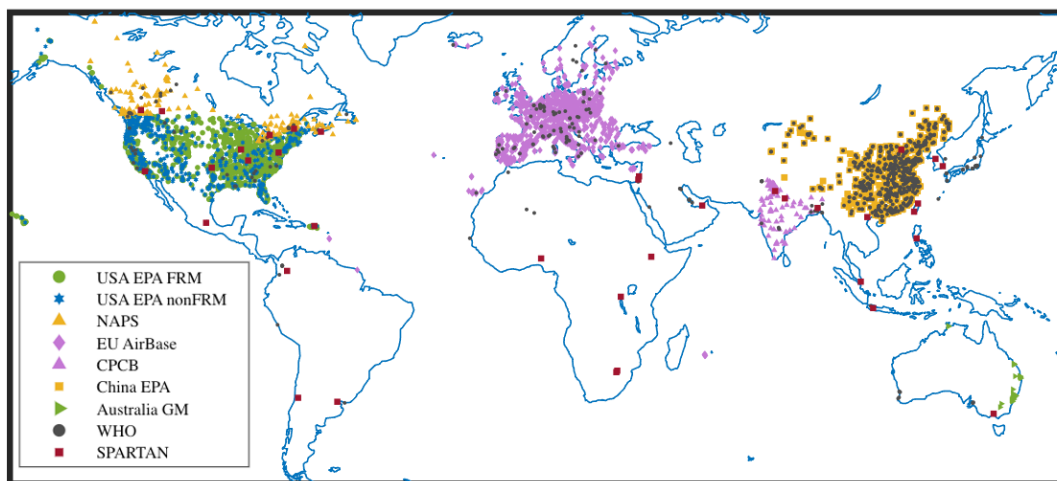
340 We simulated the global annual mean η with the GEOS-Chem chemical transport model in its high
341 performance configuration (GCHP). The simulation generally represented observed η with PWM
342 within 4% ($99.5 \mu\text{g}/\text{m}^3$ vs $95.7 \mu\text{g}/\text{m}^3$), a correlation of 0.64 over the 6,118 measurement sites, and
343 a slope of 0.81. We examined the correlation between simulation and measurements to identify
344 the two most impactful drivers for η spatial variation - aerosol composition and aerosol vertical
345 profile, both of which strongly affect the annual mean relation of columnar AOD at ambient RH
346 with surface $\text{PM}_{2.5}$ at controlled RH of 35%. We conducted sensitivity tests by eliminating the
347 spatial variation of each driver and quantified the impact on η spatial variability. Imposing a
348 globally uniform aerosol composition led to more pronounced changes (PWMD = $12.3 \mu\text{g}/\text{m}^3$)
349 reflecting how changes in aerosol composition affect both AOD and surface $\text{PM}_{2.5}$, due to the
350 effects of aerosol hygroscopicity on both quantities. Imposing a globally uniform aerosol vertical
351 profile had a moderate effect (PWMD = $8.4 \mu\text{g}/\text{m}^3$), reflecting changes in the fraction of aerosol
352 near the surface.

353 These findings motivate additional efforts to develop the simulation of aerosol composition and
354 aerosol vertical profile. Promising avenues include: (1) enhancing global long-term measurements
355 of $\text{PM}_{2.5}$ chemical composition to evaluate and improve simulations, (2) exploiting new and
356 emerging information about aerosol type from satellite remote sensing (e.g. PACE, MAIA), (3)
357 advancing simulations at finer spatial resolution to better represent processes affecting aerosol
358 composition and vertical profile, (4) leveraging aircraft, lidar, and collected AOD-to- $\text{PM}_{2.5}$
359 measurements for constraints on the vertical profile, and (5) exploiting nascent capabilities in
360 applying satellite remote sensing (e.g. TROPOMI, TEMPO, GEMS) for top-down constraints on
361 emissions that affect aerosol composition.

362

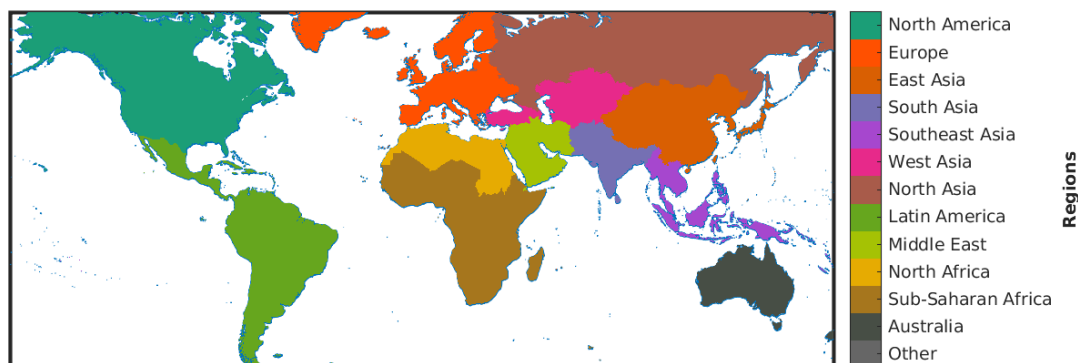


363 **Appendix**



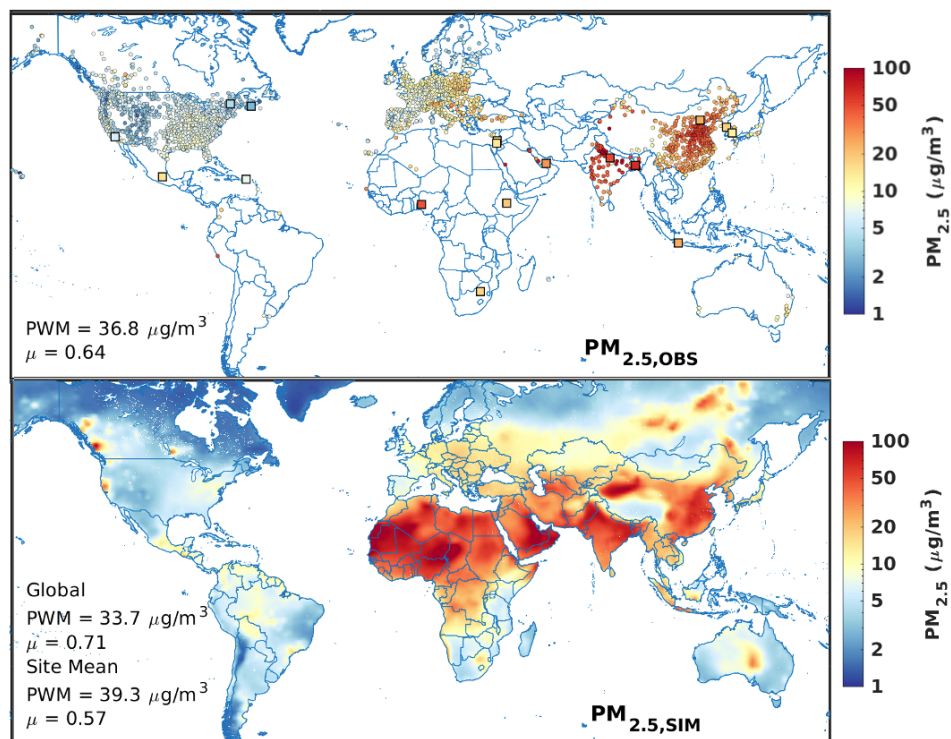
364

365 Figure A1. PM_{2.5} measurement sites from publicly available networks.



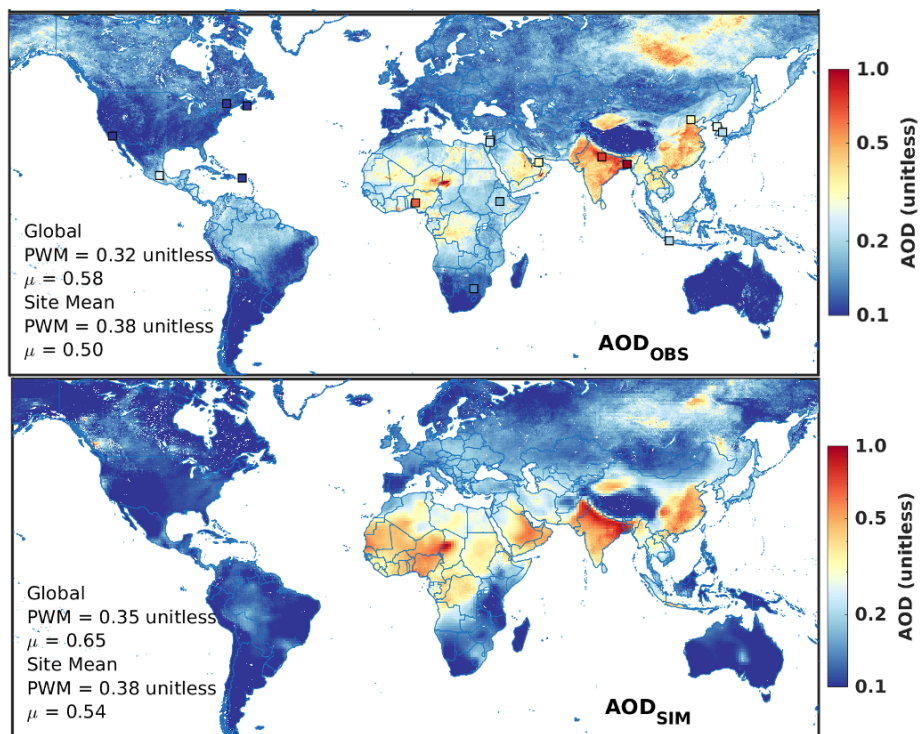
366

367 Figure A2. Region definition.



368

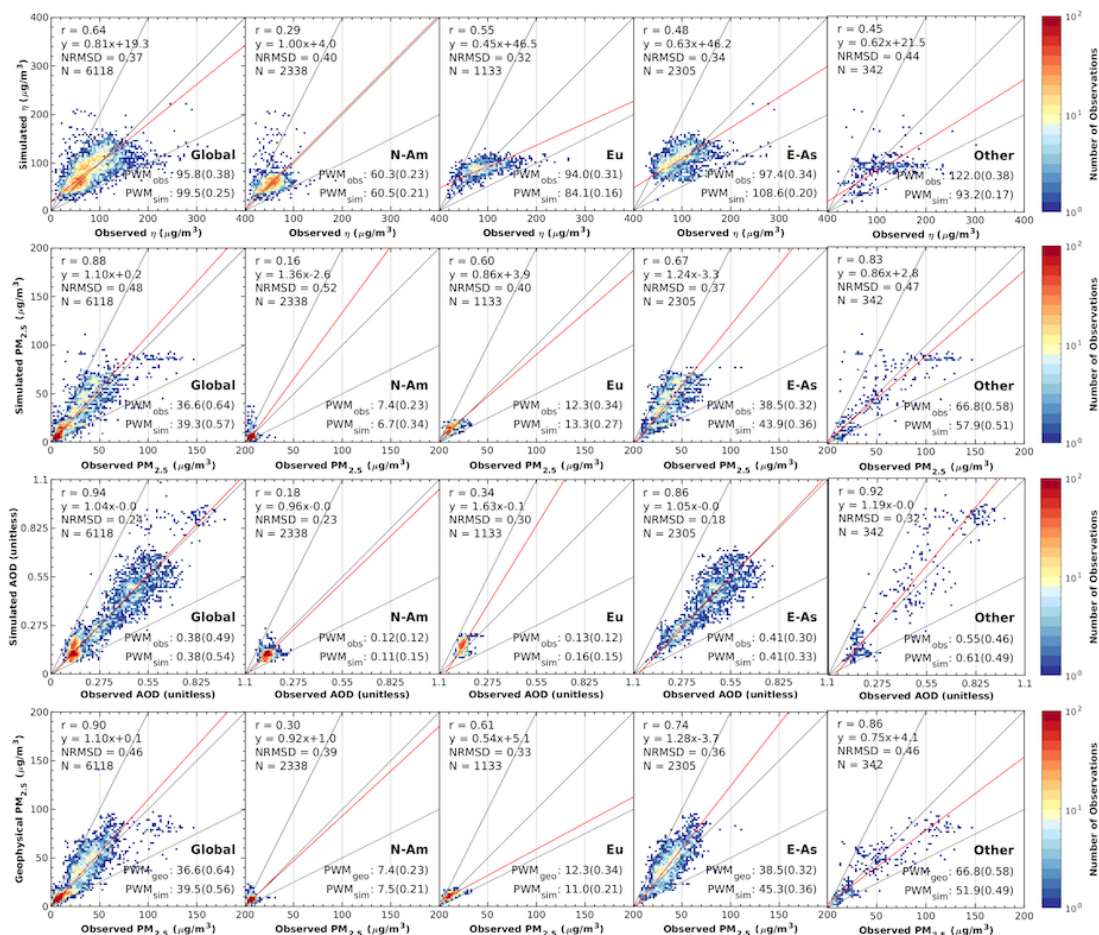
369 Figure A3. Observed (top) and simulated (bottom) annual mean $PM_{2.5}$ for 2019. Circles represent
370 measurement sites from regional networks or reported by the WHO. Squares represent measured $PM_{2.5}$
371 from SPARTAN. PWM = population-weighted mean, μ = coefficient of variation.



372

373 Figure A4. Satellite retrieved (top) and GCHP simulated (bottom) annual mean AOD for 2019. Squares
374 represent ground-measured AOD from AERONET. PWM = population-weighted mean, μ = coefficient of
375 variation.

376



377

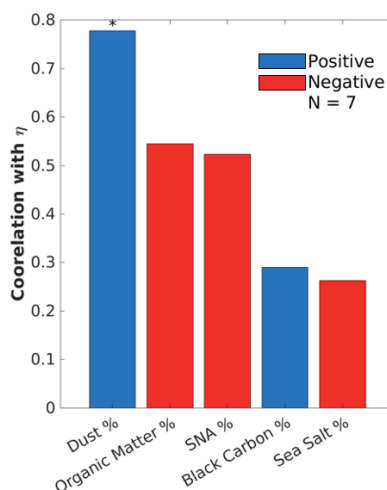
378 Figure A5. Scatter plots of simulated and observed η (top row), simulated and ground measured $\text{PM}_{2.5}$
 379 (second row), simulated and MAIAC AOD (third row), and geophysical and observed $\text{PM}_{2.5}$ (bottom
 380 row). The red line shows the line of best fit using Reduced Major Axis Linear Regression. Insets on the
 381 top left show the coefficient of determination (R^2), line of best fit, normalized root mean square deviation
 382 (NRMSD), and total number of data points (N). The bottom right insets show the population-weighted
 383 mean of observed, simulated, or geophysical estimation of each dataset, coefficients of variation are
 384 bracketed. Detailed regional mean and coefficients of variation for other regions can be found in Table
 385 A1.



386 Table A1. Regional population-weighted mean η , $PM_{2.5}$, and AOD from both observation and
 387 simulations. Geophysical $PM_{2.5}$ is also included. Coefficients of variation are bracketed. Regional mean
 388 and coefficients of variation for North America, Europe, and East Asia can be found in Figure A5.

Region	South Asia	Southeast Asia	West Asia	Latin America	Middle East	North Africa	Sub-Saharan Africa	Australia	
Number of sites	162	3	43	2	46	29	3	5	
η [$\mu\text{g}/\text{m}^3$]	Observed	121.6 (0.37)	128.6 (0.12)	154.0 (0.23)	72.0 (0.29)	94.1 (0.56)	132.3 (0.35)	196.0 (0.01)	133.9 (0.34)
	Simulated	93.4 (0.10)	82.4 (0.09)	93.4 (0.03)	74.1 (0.04)	83.6 (0.21)	126.6 (0.17)	105.9 (0.01)	187.3 (0.26)
$PM_{2.5}$ [$\mu\text{g}/\text{m}^3$]	Observed	81.0 (0.41)	35.7 (0.44)	22.0 (0.21)	12.0 (0.23)	21.7 (0.51)	28.7 (0.61)	24.0 (0.00)	35.5 (0.29)
	Simulated	70.2 (0.30)	31.8 (0.20)	20.8 (0.08)	20.9 (0.06)	10.2 (0.25)	38.3 (0.53)	16.7 (0.03)	90.0 (0.31)
	Geo-physical	62.7 (0.30)	22.7 (0.29)	13.9 (0.08)	12.4 (0.08)	20.4 (0.37)	27.3 (0.49)	12.9 (0.03)	58.1 (0.74)
AOD [unitless]	Observed	0.67 (0.25)	0.27 (0.35)	0.14 (0.08)	0.17 (0.03)	0.24 (0.21)	0.21 (0.28)	0.12 (0.01)	0.30 (0.66)
	Simulated	0.73 (0.28)	0.38 (0.18)	0.22 (0.09)	0.28 (0.02)	0.12 (0.14)	0.29 (0.32)	0.16 (0.01)	0.51 (0.26)

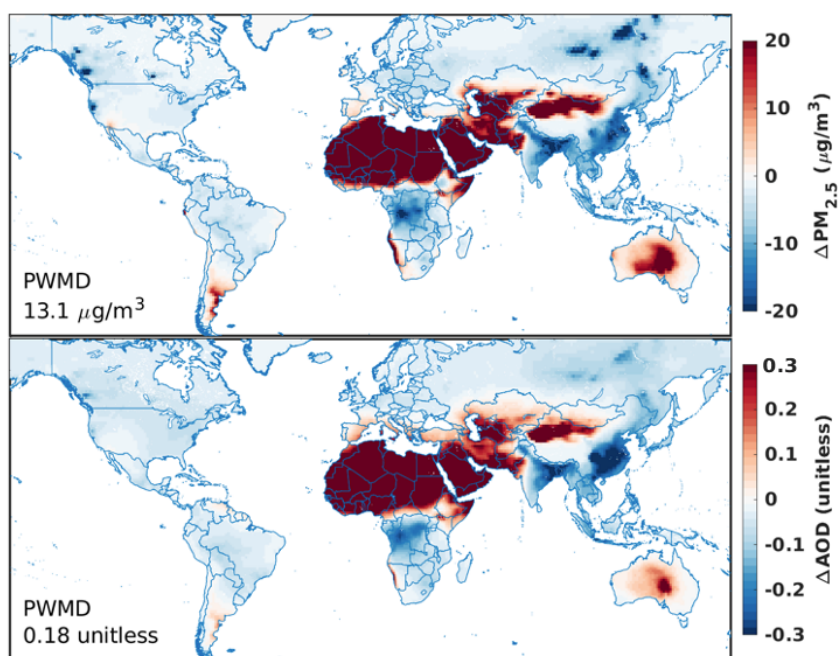
389



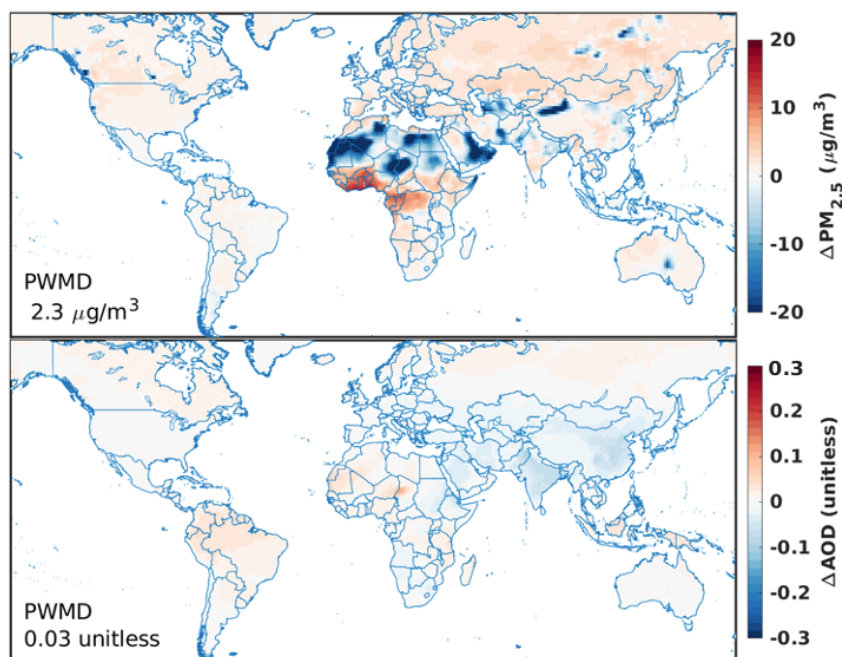
390



391 Figure A6. Correlation with η of ground-measured aerosol fractional composition from SPARTAN.
392 Organic matter is inferred through residual (Snider et al., 2016). Blue bars indicate positive correlations.
393 Red bars indicate negative correlations. Stars above each bar indicate the p-value associated with each
394 correlation. ‘***’ means the p-value is lower than 0.001, ‘**’ means lower than 0.01, and ‘*’ means
395 lower than 0.5.



396
397 Figure A7. Changes in $PM_{2.5}$ (top) and AOD (bottom) (test - base) when imposing a global PWM aerosol
398 composition.



399

400 Figure A8. Changes in PM_{2.5} (top) and AOD (bottom) (test - base) when imposing a global PWM aerosol
401 profile.

402 *Data availability.* GEOS-Chem in its high-performance configuration version 13.4.0 can be
403 downloaded at <https://zenodo.org/records/6564711>.

404 *Author contributions.* HZ and RVM designed the study. HZ performed the data analysis and model
405 simulation with contributions from AvD, CL, YL, DZ, JM, MH & IS. AvD contributed to the
406 compiled the MAIAC AOD dataset and ground-based observation datasets for PM_{2.5}. AL
407 contributed to the original MAIAC AOD dataset. CRO and XL contributed to the SPARTAN data
408 utilization and analysis. The manuscript was written by HZ and RVM with contributions from all
409 authors.

410 *Competing interests.* The authors declare no competing financial interest.

411 *Acknowledgment.* This work was supported by NASA Grant 80NSSC22K0200. We thank Dr. Mi
412 Zhou from Princeton University for providing ground based PM_{2.5} data over India.

413



414 Reference

- 415 Amos, H. M., Jacob, D. J., Holmes, C. D., Fisher, J. A., Wang, Q., Yantosca, R. M., Corbitt, E. S.,
416 Galarneau, E., Rutter, A. P., Gustin, M. S., Steffen, A., Schauer, J. J., Graydon, J. A., St Louis, V.
417 L., Talbot, R. W., Edgerton, E. S., Zhang, Y., and Sunderland, E. M.: Gas-particle partitioning of
418 atmospheric Hg(II) and its effect on global mercury deposition, *Atmospheric Chemistry and
419 Physics*, 12, 591–603, <https://doi.org/10.5194/acp-12-591-2012>, 2012.
- 420 Banerjee, T., Shitole, A. S., Mhawish, A., Anand, A., Ranjan, R., Khan, M. F., Srithawirat, T.,
421 Latif, M. T., and Mall, R. K.: Aerosol Climatology Over South and Southeast Asia: Aerosol Types,
422 Vertical Profile, and Source Fields, *Journal of Geophysical Research: Atmospheres*, 126,
423 e2020JD033554, <https://doi.org/10.1029/2020JD033554>, 2021.
- 424 Bieser, J., Aulinger, A., Matthias, V., Quante, M., and Denier Van Der Gon, H. A. C.: Vertical
425 emission profiles for Europe based on plume rise calculations, *Environmental Pollution*, 159,
426 2935–2946, <https://doi.org/10.1016/J.ENVPOL.2011.04.030>, 2011.
- 427 Burnett, R., Chen, H., Szyszkowicz, M., Fann, N., Hubbell, B., Pope, C. A., Apte, J. S., Brauer,
428 M., Cohen, A., Weichenthal, S., Coggins, J., Di, Q., Brunekreef, B., Frostad, J., Lim, S. S., Kan,
429 H., Walker, K. D., Thurston, G. D., Hayes, R. B., Lim, C. C., Turner, M. C., Jerrett, M., Krewski,
430 D., Gapstur, S. M., Diver, W. R., Ostro, B., Goldberg, D., Crouse, D. L., Martin, R. V., Peters, P.,
431 Pinault, L., Tjepkema, M., Van Donkelaar, A., Villeneuve, P. J., Miller, A. B., Yin, P., Zhou, M.,
432 Wang, L., Janssen, N. A. H., Marra, M., Atkinson, R. W., Tsang, H., Thach, T. Q., Cannon, J. B.,
433 Allen, R. T., Hart, J. E., Laden, F., Cesaroni, G., Forastiere, F., Weinmayr, G., Jaensch, A., Nagel,
434 G., Concin, H., and Spadaro, J. V.: Global estimates of mortality associated with longterm
435 exposure to outdoor fine particulate matter, *Proceedings of the National Academy of Sciences of
436 the United States of America*, 115, 9592–9597, <https://doi.org/10.1073/pnas.1803222115>, 2018.
- 437 Canagaratna, M. R., Jimenez, J. L., Kroll, J. H., Chen, Q., Kessler, S. H., Massoli, P., Hildebrandt
438 Ruiz, L., Fortner, E., Williams, L. R., Wilson, K. R., Surratt, J. D., Donahue, N. M., Jayne, J. T.,
439 and Worsnop, D. R.: Elemental ratio measurements of organic compounds using aerosol mass
440 spectrometry: Characterization, improved calibration, and implications, *Atmospheric Chemistry
441 and Physics*, 15, 253–272, <https://doi.org/10.5194/acp-15-253-2015>, 2015.
- 442 Center for International Earth Science Information Network - CIESIN - Columbia University:
443 Gridded Population of the World, Version 4 (GPWv4): Population Density, Revision 11, 2018.
- 444 Christidis, T., Erickson, A. C., Pappin, A. J., Crouse, D. L., Pinault, L. L., Weichenthal, S. A.,
445 Brook, J. R., van Donkelaar, A., Hystad, P., Martin, R. V., Tjepkema, M., Burnett, R. T., and
446 Brauer, M.: Low concentrations of fine particle air pollution and mortality in the Canadian
447 Community Health Survey cohort, *Environmental Health*, 18, 84, [https://doi.org/10.1186/s12940-
448 019-0518-y](https://doi.org/10.1186/s12940-019-0518-y), 2019.
- 449 Chu, D. A., Ferrare, R., Szykman, J., Lewis, J., Scarino, A., Hains, J., Burton, S., Chen, G., Tsai,
450 T., Hostetler, C., Hair, J., Holben, B., and Crawford, J.: Regional characteristics of the relationship
451 between columnar AOD and surface PM_{2.5}: Application of lidar aerosol extinction profiles over



- 452 Baltimore-Washington Corridor during DISCOVER-AQ, *Atmospheric Environment*, 101,
453 338e349-349, <https://doi.org/10.1016/j.atmosenv.2014.11.034>, 2015.
- 454 Cohen, A. J., Brauer, M., Burnett, R., Anderson, H. R., Frostad, J., Estep, K., Balakrishnan, K.,
455 Brunekreef, B., Dandona, L., Dandona, R., Feigin, V., Freedman, G., Hubbell, B., Jobling, A., Kan,
456 H., Knibbs, L., Liu, Y., Martin, R., Morawska, L., Pope, C. A., Shin, H., Straif, K., Shaddick, G.,
457 Thomas, M., van Dingenen, R., van Donkelaar, A., Vos, T., Murray, C. J. L., and Forouzanfar, M.
458 H.: Estimates and 25-year trends of the global burden of disease attributable to ambient air
459 pollution: an analysis of data from the Global Burden of Diseases Study 2015, *The Lancet*, 389,
460 1907–1918, [https://doi.org/10.1016/S0140-6736\(17\)30505-6](https://doi.org/10.1016/S0140-6736(17)30505-6), 2017.
- 461 Damascena, A. S., Yamasoe, M. A., Martins, V. S., Rosas, J., Benavente, N. R., Sánchez, M. P.,
462 Tanaka, N. I., and Saldiva, P. H. N.: Exploring the relationship between high-resolution aerosol
463 optical depth values and ground-level particulate matter concentrations in the Metropolitan Area
464 of São Paulo, *Atmospheric Environment*, 244, 117949,
465 <https://doi.org/10.1016/j.atmosenv.2020.117949>, 2021.
- 466 Di, Q., Kloog, I., Koutrakis, P., Lyapustin, A., Wang, Y., and Schwartz, J.: Assessing PM_{2.5}
467 Exposures with High Spatiotemporal Resolution across the Continental United States,
468 *Environmental Science and Technology*, 50, 4712–4721, <https://doi.org/10.1021/acs.est.5b06121>,
469 2016.
- 470 van Donkelaar, A., Martin, R. V., and Park, R. J.: Estimating ground-level PM_{2.5} using aerosol
471 optical depth determined from satellite remote sensing, *Journal of Geophysical Research*
472 *Atmospheres*, 111, 1–10, <https://doi.org/10.1029/2005JD006996>, 2006.
- 473 van Donkelaar, A., Martin, R. V., Brauer, M., Kahn, R., Levy, R., Verduzco, C., and Villeneuve,
474 P. J.: Global estimates of ambient fine particulate matter concentrations from satellite-based
475 aerosol optical depth: Development and application, *Environmental Health Perspectives*, 118,
476 847–855, <https://doi.org/10.1289/ehp.0901623>, 2010.
- 477 van Donkelaar, A., Martin, R. V., Spurr, R. J. D., Drury, E., Remer, L. A., Levy, R. C., and Wang,
478 J.: Optimal estimation for global ground-level fine particulate matter concentrations, *Journal of*
479 *Geophysical Research Atmospheres*, 118, 5621–5636, <https://doi.org/10.1002/jgrd.50479>, 2013.
- 480 van Donkelaar, A., Martin, R. V., Spurr, R. J. D., and Burnett, R. T.: High-Resolution Satellite-
481 Derived PM_{2.5} from Optimal Estimation and Geographically Weighted Regression over North
482 America, *Environmental Science and Technology*, 49, 10482–10491,
483 <https://doi.org/10.1021/acs.est.5b02076>, 2015.
- 484 van Donkelaar, A., Martin, R. V., Brauer, M., Hsu, N. C., Kahn, R. A., Levy, R. C., Lyapustin, A.,
485 Sayer, A. M., and Winker, D. M.: Global Estimates of Fine Particulate Matter using a Combined
486 Geophysical-Statistical Method with Information from Satellites, Models, and Monitors,
487 *Environmental Science and Technology*, 50, 3762–3772, <https://doi.org/10.1021/acs.est.5b05833>,
488 2016.



- 489 Eastham, S. D., Long, M. S., Keller, C. A., Lundgren, E., Yantosca, R. M., Zhuang, J., Li, C., Lee,
490 C. J., Yannetti, M., Auer, B. M., Clune, T. L., Kouatchou, J., Putman, W. M., Thompson, M. A.,
491 Trayanov, A. L., Molod, A. M., Martin, R. V., and Jacob, D. J.: GEOS-Chem high performance
492 (GCHP v11-02c): A next-generation implementation of the GEOS-Chem chemical transport
493 model for massively parallel applications, *Geoscientific Model Development*, 11, 2941–2953,
494 <https://doi.org/10.5194/gmd-11-2941-2018>, 2018.
- 495 Fairlie, D. T., Jacob, D. J., and Park, R. J.: The impact of transpacific transport of mineral dust in
496 the United States, *Atmospheric Environment*, 41, 1251–1266,
497 <https://doi.org/10.1016/j.atmosenv.2006.09.048>, 2007.
- 498 Ford, B. and Heald, C. L.: Exploring the uncertainty associated with satellite-based estimates of
499 premature mortality due to exposure to fine particulate matter, *Atmospheric Chemistry and Physics*
500 *Discussions*, 15, 25329–25380, <https://doi.org/10.5194/acpd-15-25329-2015>, 2015.
- 501 Fountoukis, C. and Nenes, A.: ISORROPIAII: A computationally efficient thermodynamic
502 equilibrium model for K^+ - Ca^{2+} - Mg^{2+} - NH_4^+ - Na^+ - SO_4^{2-} - NO_3^- - Cl^- - H_2O aerosols, *Atmospheric*
503 *Chemistry and Physics*, 7, 4639–4659, <https://doi.org/10.5194/acp-7-4639-2007>, 2007.
- 504 Giles, D. M., Sinyuk, A., Sorokin, M. G., Schafer, J. S., Smirnov, A., Slutsker, I., Eck, T. F.,
505 Holben, B. N., Lewis, J. R., Campbell, J. R., Welton, E. J., Korokin, S. V., and Lyapustin, A. I.:
506 Advancements in the Aerosol Robotic Network (AERONET) Version 3 database - Automated
507 near-real-time quality control algorithm with improved cloud screening for Sun photometer
508 aerosol optical depth (AOD) measurements, *Atmospheric Measurement Techniques*, 12, 169–209,
509 <https://doi.org/10.5194/amt-12-169-2019>, 2019.
- 510 Guo, J., Xia, F., Zhang, Y., Liu, H., Li, J., Lou, M., He, J., Yan, Y., Wang, F., Min, M., and Zhai,
511 P.: Impact of diurnal variability and meteorological factors on the $PM_{2.5}$ - AOD relationship:
512 Implications for $PM_{2.5}$ remote sensing, *Environmental Pollution*, 221, 94–104,
513 <https://doi.org/10.1016/j.envpol.2016.11.043>, 2017.
- 514 Gupta, P., Christopher, S. A., Wang, J., Gehrig, R., Lee, Y., and Kumar, N.: Satellite remote
515 sensing of particulate matter and air quality assessment over global cities, *Atmospheric*
516 *Environment*, 40, 5880–5892, <https://doi.org/10.1016/j.atmosenv.2006.03.016>, 2006.
- 517 Hammer, M. S., Martin, R. V., Van Donkelaar, A., Buchard, V., Torres, O., Ridley, D. A., and
518 Spurr, R. J. D.: Interpreting the ultraviolet aerosol index observed with the OMI satellite
519 instrument to understand absorption by organic aerosols: Implications for atmospheric oxidation
520 and direct radiative effects, *Atmospheric Chemistry and Physics*, 16, 2507–2523,
521 <https://doi.org/10.5194/acp-16-2507-2016>, 2016.
- 522 Hao, H., Wang, Y., Zhu, Q., Zhang, H., Rosenberg, A., Schwartz, J., Amini, H., van Donkelaar,
523 A., Martin, R., Liu, P., Weber, R., Russel, A., Yitshak-sade, M., Chang, H., and Shi, L.: National
524 Cohort Study of Long-Term Exposure to $PM_{2.5}$ Components and Mortality in Medicare American
525 Older Adults, *Environ. Sci. Technol.*, 57, 6835–6843, <https://doi.org/10.1021/acs.est.2c07064>,
526 2023.



- 527 He, Q., Wang, M., and Yim, S. H. L.: The spatiotemporal relationship between PM_{2.5} and aerosol
528 optical depth in China: Influencing factors and implications for satellite PM_{2.5} estimations using
529 MAIAC aerosol optical depth, *Atmospheric Chemistry and Physics*, 21, 18375–18391,
530 <https://doi.org/10.5194/acp-21-18375-2021>, 2021.
- 531 Heald, C. L., Collett, J. L., Lee, T., Benedict, K. B., Schwandner, F. M., Li, Y., Clarisse, L.,
532 Hurtmans, D. R., Van Damme, M., Clerbaux, C., Coheur, P. F., Philip, S., Martin, R. V., and Pye,
533 H. O. T.: Atmospheric ammonia and particulate inorganic nitrogen over the United States,
534 *Atmospheric Chemistry and Physics*, 12, 10295–10312, <https://doi.org/10.5194/acp-12-10295-535>
535 2012, 2012.
- 536 Hu, X., Waller, L. A., Lyapustin, A., Wang, Y., and Liu, Y.: 10-year spatial and temporal trends
537 of PM_{2.5} concentrations in the southeastern US estimated using high-resolution satellite data,
538 *Atmospheric Chemistry and Physics*, 14, 6301–6314, <https://doi.org/10.5194/acp-14-6301-2014>,
539 2014.
- 540 Jaeglé, L., Quinn, P. K., Bates, T. S., Alexander, B., and Lin, J. T.: Global distribution of sea salt
541 aerosols: New constraints from in situ and remote sensing observations, *Atmospheric Chemistry
542 and Physics*, 11, 3137–3157, <https://doi.org/10.5194/acp-11-3137-2011>, 2011.
- 543 Jin, Q., Crippa, P., and Pryor, S. C.: Spatial characteristics and temporal evolution of the
544 relationship between PM_{2.5} and aerosol optical depth over the eastern USA during 2003–2017,
545 *Atmospheric Environment*, 239, 117718, <https://doi.org/10.1016/j.atmosenv.2020.117718>, 2020.
- 546 Jin, X., Fiore, A. M., Curci, G., Lyapustin, A., Civerolo, K., Ku, M., Van Donkelaar, A., and
547 Martin, R. V.: Assessing uncertainties of a geophysical approach to estimate surface fine
548 particulate matter distributions from satellite-observed aerosol optical depth, *Atmospheric
549 Chemistry and Physics*, 19, 295–313, <https://doi.org/10.5194/acp-19-295-2019>, 2019.
- 550 Kondragunta, S., Veihelmann, B., and Chatfield, R. J.: Monitoring Surface PM_{2.5}: An
551 International Constellation Approach to Enhancing the Role of Satellite Observations,
552 <https://doi.org/10.25923/7SNZ-VN34>, 2022.
- 553 Kopke P., H. M. S. I. S. E. P.: Aerosol data set, Max Planck Institut fur Meteorologie, Report No.
554 243, Max-Planck-Institut Fur Meteorologie, Hamburg, <https://doi.org/Report No. 243>, 1997.
- 555 Latimer, R. N. C. and Martin, R. V.: Interpretation of measured aerosol mass scattering efficiency
556 over North America using a chemical transport model, *Atmospheric Chemistry and Physics*, 19,
557 2635–2653, <https://doi.org/10.5194/acp-19-2635-2019>, 2019.
- 558 Li, J., Carlson, B. E., and Laci, A. A.: How well do satellite AOD observations represent the
559 spatial and temporal variability of PM_{2.5} concentration for the United States?, *Atmospheric
560 Environment*, 102, 260–273, <https://doi.org/10.1016/j.atmosenv.2014.12.010>, 2015.
- 561 Li, Y., Martin, R. V., Li, C., Boys, B. L., van Donkelaar, A., Meng, J., and Pierce, J. R.:
562 Development and evaluation of processes affecting simulation of diel fine particulate matter



- 563 variation in the GEOS-Chem model, *Atmospheric Chemistry and Physics*, 23, 12525–12543,
564 <https://doi.org/10.5194/ACP-23-12525-2023>, 2023.
- 565 Liu, H., Jacob, D. J., Bey, I., and Yantosca, R. M.: Constraints from ^{210}Pb and ^7Be on wet
566 deposition and transport in a global three-dimensional chemical tracer model driven by assimilated
567 meteorological fields, *Journal of Geophysical Research Atmospheres*, 106, 12109–12128,
568 <https://doi.org/10.1029/2000JD900839>, 2001.
- 569 Liu, X., Turner, J. R., Hand, J. L., Schichtel, B. A., and Martin, R. V.: A Global-Scale Mineral
570 Dust Equation, *Journal of Geophysical Research: Atmospheres*, 127, e2022JD036937,
571 <https://doi.org/10.1029/2022JD036937>, 2022.
- 572 Liu, X., Turner, J. R., Oxford, C. R., McNeill, J., Walsh, B., Le Roy, E., Weagle, C. L., Stone, E.,
573 Zhu, H., Liu, W., Wei, Z., Hyslop, N. P., Giacomo, J., Dillner, A. M., Salam, A., Hossen, A., Islam,
574 Z., Abboud, I., Akoshile, C., Amador-Muñoz, O., Anh, N. X., Asfaw, A., Balasubramanian, R.,
575 Chang, R. Y.-W., Coburn, C., Dey, S., Diner, D. J., Dong, J., Farrah, T., Gahungu, P., Garland, R.
576 M., Grutter de la Mora, M., Hasheminassab, S., John, J., Kim, J., Kim, J. S., Langerman, K., Lee,
577 P.-C., Lestari, P., Liu, Y., Mamo, T., Martins, M., Mayol-Bracero, O. L., Naidoo, M., Park, S. S.,
578 Schechner, Y., Schofield, R., Tripathi, S. N., Windwer, E., Wu, M.-T., Zhang, Q., Brauer, M.,
579 Rudich, Y., and Martin, R. V.: Elemental Characterization of Ambient Particulate Matter for a
580 Globally Distributed Monitoring Network: Methodology and Implications, *ACS EST Air*,
581 <https://doi.org/10.1021/acsestair.3c00069>, 2024.
- 582 Lyapustin, A., Wang, Y., Korkin, S., and Huang, D.: MODIS Collection 6 MAIAC algorithm,
583 *Atmospheric Measurement Techniques*, 11, 5741–5765, [https://doi.org/10.5194/amt-11-5741-](https://doi.org/10.5194/amt-11-5741-2018)
584 2018, 2018.
- 585 Martin, R. V., Jacob, D. J., Yantosca, R. M., Chin, M., and Ginoux, P.: Global and regional
586 decreases in tropospheric oxidants from photochemical effects of aerosols, *Journal of Geophysical*
587 *Research: Atmospheres*, 108, <https://doi.org/10.1029/2002jd002622>, 2003.
- 588 Martin, R. V., Brauer, M., van Donkelaar, A., Shaddick, G., Narain, U., and Dey, S.: No one knows
589 which city has the highest concentration of fine particulate matter, *Atmospheric Environment: X*,
590 3, <https://doi.org/10.1016/j.aeaoa.2019.100040>, 2019.
- 591 Martin, R. V., Eastham, S. D., Bindle, L., Lundgren, E. W., Clune, T. L., Keller, C. A., Downs,
592 W., Zhang, D., Lucchesi, R. A., Sulprizio, M. P., Yantosca, R. M., Li, Y., Estrada, L., Putman, W.
593 M., Auer, B. M., Trayanov, L., Pawson, S., and Jacob, D. J.: Improved Advection , Resolution ,
594 Performance , and Community Access in the New Generation (Version 13) of the High
595 Performance GEOS-Chem Global Atmospheric Chemistry Model (GCHP), *Geoscientific Model*
596 *Development Discussions*, 720, 1–30, <https://doi.org/10.5194/gmd-2022-42>, 2022.
- 597 McDuffie, E. E., Smith, S. J., O'Rourke, P., Tibrewal, K., Venkataraman, C., Marais, E. A., Zheng,
598 B., Crippa, M., Brauer, M., and Martin, R. V.: A global anthropogenic emission inventory of
599 atmospheric pollutants from sector- And fuel-specific sources (1970-2017): An application of the
600 Community Emissions Data System (CEDS), *Earth System Science Data*, 12, 3413–3442,
601 <https://doi.org/10.5194/essd-12-3413-2020>, 2020.



- 602 Meng, J., Martin, R. V., Ginoux, P., Hammer, M., Sulprizio, M. P., Ridley, D. A., and Van
603 Donkelaar, A.: Grid-independent high-resolution dust emissions (v1.0) for chemical transport
604 models: Application to GEOS-Chem (12.5.0), *Geoscientific Model Development*, 14, 4249–4260,
605 <https://doi.org/10.5194/gmd-14-4249-2021>, 2021.
- 606 Miao, R., Chen, Q., Zheng, Y., Cheng, X., Sun, Y., Palmer, P. I., Shrivastava, M., Guo, J., Zhang,
607 Q., Liu, Y., Tan, Z., Ma, X., Chen, S., Zeng, L., Lu, K., and Zhang, Y.: Model bias in simulating
608 major chemical components of PM_{2.5} in China, *Atmospheric Chemistry and Physics*, 20, 12265–
609 12284, <https://doi.org/10.5194/acp-20-12265-2020>, 2020.
- 610 Murray, C. J. L., Aravkin, A. Y., Zheng, P., Abbafati, C., Abbas, K. M., Abbasi-Kangevari, M.,
611 Abd-Allah, F., Abdelalim, A., Abdollahi, M., Abdollahpour, I., Abegaz, K. H., Abolhassani, H.,
612 Aboyans, V., Abreu, L. G., Abrigo, M. R. M., Abualhasan, A., Abu-Raddad, L. J., Abushouk, A.
613 I., Adabi, M., Adekanmbi, V., Adeoye, A. M., Adetokunboh, O. O., Adham, D., Advani, S. M.,
614 Agarwal, G., Aghamir, S. M. K., Agrawal, A., Ahmad, T., Ahmadi, K., Ahmadi, M., Ahmadieh,
615 H., Ahmed, M. B., Akalu, T. Y., Akinyemi, R. O., Akinyemiju, T., Akombi, B., Akunna, C. J.,
616 Alahdab, F., Al-Aly, Z., Alam, K., Alam, S., Alam, T., Alanezi, F. M., Alanzi, T. M., Alemu, B.
617 wassihun, Alhabib, K. F., Ali, M., Ali, S., Alicandro, G., Alinia, C., Alipour, V., Alizade, H.,
618 Aljunid, S. M., Alla, F., Allebeck, P., Almasi-Hashiani, A., Al-Mekhlafi, H. M., Alonso, J.,
619 Altirkawi, K. A., Amini-Rarani, M., Amiri, F., Amugsi, D. A., Ancuceanu, R., Anderlini, D.,
620 Anderson, J. A., Andrei, C. L., Andrei, T., Angus, C., Anjomshoa, M., Ansari, F., Ansari-
621 Moghaddam, A., Antonazzo, I. C., Antonio, C. A. T., Antony, C. M., Antriyandarti, E., Anvari,
622 D., Anwer, R., Appiah, S. C. Y., Arabloo, J., Arab-Zozani, M., Ariani, F., Armoon, B., Ärnlöv, J.,
623 Arzani, A., Asadi-Aliabadi, M., Asadi-Pooya, A. A., Ashbaugh, C., Assmus, M., Atafar, Z., Atnafu,
624 D. D., Atout, M. M. W., Ausloos, F., Ausloos, M., Quintanilla, B. P. A., Ayano, G., Ayanore, M.
625 A., Azari, S., Azarian, G., Azene, Z. N., et al.: Global burden of 87 risk factors in 204 countries
626 and territories, 1990–2019: a systematic analysis for the Global Burden of Disease Study 2019,
627 *The Lancet*, 396, 1223–1249, [https://doi.org/10.1016/S0140-6736\(20\)30752-2](https://doi.org/10.1016/S0140-6736(20)30752-2), 2020.
- 628 Nguyen, T. T. N., Pham, H. V., Lasko, K., Bui, M. T., Laffly, D., Jourdan, A., and Bui, H. Q.:
629 Spatiotemporal analysis of ground and satellite-based aerosol for air quality assessment in the
630 Southeast Asia region, *Environmental Pollution*, 255, 113106,
631 <https://doi.org/10.1016/j.envpol.2019.113106>, 2019.
- 632 Pai, S. J., Heald, C. L., Pierce, J. R., Farina, S. C., Marais, E. A., Jimenez, J. L., Campuzano-Jost,
633 P., Nault, B. A., Middlebrook, A. M., Coe, H., Shilling, J. E., Bahreini, R., Dingle, J. H., and Vu,
634 K.: An evaluation of global organic aerosol schemes using airborne observations, *Atmospheric
635 Chemistry and Physics*, 20, 2637–2665, <https://doi.org/10.5194/acp-20-2637-2020>, 2020.
- 636 Park, R. J., Jacob, D. J., Chin, M., and Martin, R. V.: Sources of carbonaceous aerosols over the
637 United States and implications for natural visibility, *Journal of Geophysical Research
638 Atmospheres*, 108, <https://doi.org/10.1029/2002jd003190>, 2003.
- 639 Philip, S., Martin, R. V., Pierce, J. R., Jimenez, J. L., Zhang, Q., Canagaratna, M. R., Spracklen,
640 D. V., Nowlan, C. R., Lamsal, L. N., Cooper, M. J., and Krotkov, N. A.: Spatially and seasonally



- 641 resolved estimate of the ratio of organic mass to organic carbon, *Atmospheric Environment*, 48,
642 34–40, <https://doi.org/10.1016/j.atmosenv.2013.11.065>, 2014.
- 643 Philip, S., Martin, R. V., Snider, G., Weagle, C. L., Van Donkelaar, A., Brauer, M., Henze, D. K.,
644 Klimont, Z., Venkataraman, C., Guttikunda, S. K., and Zhang, Q.: Anthropogenic fugitive,
645 combustion and industrial dust is a significant, underrepresented fine particulate matter source in
646 global atmospheric models, *Environmental Research Letters*, 12, <https://doi.org/10.1088/1748-9326/aa65a4>, 2017.
- 648 Pinault, L., Tjepkema, M., Crouse, D. L., Weichenthal, S., van Donkelaar, A., Martin, R. V.,
649 Brauer, M., Chen, H., and Burnett, R. T.: Risk estimates of mortality attributed to low
650 concentrations of ambient fine particulate matter in the Canadian community health survey cohort,
651 *Environmental Health*, 15, 18, <https://doi.org/10.1186/s12940-016-0111-6>, 2016.
- 652 Sayer, A. M., Munchak, L. A., Hsu, N. C., Levy, R. C., Bettenhausen, C., and Jeong, M. J.: MODIS
653 Collection 6 aerosol products: Comparison between Aqua’s e-Deep Blue, Dark Target, and
654 “merged” data sets, and usage recommendations, *Journal of Geophysical Research: Atmospheres*,
655 119, 13,965–13,989, <https://doi.org/10.1002/2014JD022453>, 2014.
- 656 Schubert, S. D., Rood, R. B., and Pfendtner, J.: An Assimilated Dataset for Earth Science
657 Applications, *Bulletin of the American Meteorological Society*, 74, 2331–2342,
658 [https://doi.org/10.1175/1520-0477\(1993\)074<2331:AADFES>2.0.CO;2](https://doi.org/10.1175/1520-0477(1993)074<2331:AADFES>2.0.CO;2), 1993.
- 659 Shimadera, H., Hayami, H., Chatani, S., Morino, Y., Mori, Y., Morikawa, T., Yamaji, K., and
660 Ohara, T.: Sensitivity analyses of factors influencing CMAQ performance for fine particulate
661 nitrate, *Journal of the Air & Waste Management Association*, 64, 374–387,
662 <https://doi.org/10.1080/10962247.2013.778919>, 2014.
- 663 Snider, G., Weagle, C. L., Murdymootoo, K. K., Ring, A., Ritchie, Y., Stone, E., Walsh, A.,
664 Akoshile, C., Anh, N. X., Balasubramanian, R., Brook, J., Qonitan, F. D., Dong, J., Griffith, D.,
665 He, K., Holben, B. N., Kahn, R., Lagrosas, N., Lestari, P., Ma, Z., Misra, A., Norford, L. K., Quel,
666 E. J., Salam, A., Schichtel, B., Segev, L., Tripathi, S., Wang, C., Yu, C., Zhang, Q., Zhang, Y.,
667 Brauer, M., Cohen, A., Gibson, M. D., Liu, Y., Martins, J. V., Rudich, Y., and Martin, R. V.:
668 Variation in global chemical composition of PM_{2.5}: emerging results from SPARTAN,
669 *Atmospheric Chemistry and Physics*, 16, 9629–9653, <https://doi.org/10.5194/acp-16-9629-2016>,
670 2016.
- 671 Travis, K. R., Crawford, J. H., Chen, G., Jordan, C. E., Nault, B. A., Kim, H., Jimenez, J. L.,
672 Campuzano-Jost, P., Dibb, J. E., Woo, J. H., Kim, Y., Zhai, S., Wang, X., McDuffie, E. E., Luo,
673 G., Yu, F., Kim, S., Simpson, I. J., Blake, D. R., Chang, L., and Kim, M. J.: Limitations in
674 representation of physical processes prevent successful simulation of PM_{2.5} during KORUS-AQ,
675 *Atmospheric Chemistry and Physics*, 22, 7933–7958, <https://doi.org/10.5194/acp-22-7933-2022>,
676 2022.
- 677 Wang, Q., Jacob, D. J., Spackman, J. R., Perring, A. E., Schwarz, J. P., Moteki, N., Marais, E. A.,
678 Ge, C., Wang, J., and Barrett, S. R. H.: Global budget and radiative forcing of black carbon aerosol:



- 679 Constraints from pole-to-pole (HIPPO) observations across the Pacific, *Journal of Geophysical*
680 *Research*, 119, 195–206, <https://doi.org/10.1002/2013JD020824>, 2014.
- 681 Wang, Y., Jacob, D. J., and Logan, J. A.: Global simulation of tropospheric O₃-NO_x-hydrocarbon
682 chemistry - 1. Model formulation, *Journal of Geophysical Research: Atmospheres*, 103, 10713–
683 10725, <https://doi.org/10.1029/98jd00158>, 1998.
- 684 Weichenthal, S., Pinault, L., Christidis, T., Burnett, R. T., Brook, J. R., Chu, Y., Crouse, D. L.,
685 Erickson, A. C., Hystad, P., Li, C., Martin, R. V., Meng, J., Pappin, A. J., Tjepkema, M., van
686 Donkelaar, A., Weagle, C. L., and Brauer, M.: How low can you go? Air pollution affects mortality
687 at very low levels, *Science Advances*, 8, eabo3381, <https://doi.org/10.1126/sciadv.abo3381>, 2022.
- 688 Wendt, E. A., Ford, B., Cheeseman, M., Rosen, Z., Pierce, J. R., H. Jathar, S., L'Orange, C., Quinn,
689 C., Long, M., Mehaffy, J., D. Miller-Lionberg, D., H. Hagan, D., and Volckens, J.: A national
690 crowdsourced network of low-cost fine particulate matter and aerosol optical depth monitors:
691 results from the 2021 wildfire season in the United States, *Environmental Science: Atmospheres*,
692 3, 1563–1575, <https://doi.org/10.1039/D3EA00086A>, 2023.
- 693 Weng, H., Lin, J., Martin, R., Millet, D. B., Jaeglé, L., Ridley, D., Keller, C., Li, C., Du, M., and
694 Meng, J.: Global high-resolution emissions of soil NO_x, sea salt aerosols, and biogenic volatile
695 organic compounds, *Scientific Data*, 7, 1–15, <https://doi.org/10.1038/s41597-020-0488-5>, 2020.
- 696 van der Werf, G. R., Randerson, J. T., Giglio, L., Van Leeuwen, T. T., Chen, Y., Rogers, B. M.,
697 Mu, M., Van Marle, M. J. E., Morton, D. C., Collatz, G. J., Yokelson, R. J., and Kasibhatla, P. S.:
698 Global fire emissions estimates during 1997–2016, *Earth System Science Data*, 9, 697–720,
699 <https://doi.org/10.5194/essd-9-697-2017>, 2017.
- 700 White, W. H., Trzepla, K., Hyslop, N. P., and Schichtel, B. A.: A critical review of filter
701 transmittance measurements for aerosol light absorption, and de novo calibration for a decade of
702 monitoring on PTFE membranes, *Aerosol Science and Technology*, 50, 984–1002,
703 <https://doi.org/10.1080/02786826.2016.1211615>, 2016.
- 704 Xin, J., Zhang, Q., Wang, L., Gong, C., Wang, Y., Liu, Z., and Gao, W.: The empirical relationship
705 between the PM_{2.5} concentration and aerosol optical depth over the background of North China
706 from 2009 to 2011, *Atmospheric Research*, 138, 179–188,
707 <https://doi.org/10.1016/j.atmosres.2013.11.001>, 2014.
- 708 Yang, Q., Yuan, Q., Yue, L., Li, T., Shen, H., and Zhang, L.: The relationships between PM_{2.5}
709 and aerosol optical depth (AOD) in mainland China: About and behind the spatio-temporal
710 variations, *Environmental Pollution*, 248, 526–535, <https://doi.org/10.1016/j.envpol.2019.02.071>,
711 2019.
- 712 Zakoura, M. and Pandis, S. N.: Overprediction of aerosol nitrate by chemical transport models:
713 The role of grid resolution, *Atmospheric Environment*, 187, 390–400,
714 <https://doi.org/10.1016/J.ATMOSENV.2018.05.066>, 2018.



- 715 Zhai, S., Jacob, D., Brewer, J., Li, K., Moch, J., Kim, J., Lee, S., Lim, H., Lee, H. C., Kuk, S. K.,
716 Park, R., Jeong, J., Wang, X., Liu, P., Luo, G., Yu, F., Meng, J., Martin, R., Travis, K., Hair, J.,
717 Anderson, B., Dibb, J., Jimenez, J., Campuzano-Jost, P., Nault, B., Woo, J.-H., Kim, Y., Zhang,
718 Q., and Liao, H.: Interpretation of geostationary satellite aerosol optical depth (AOD) over East
719 Asia in relation to fine particulate matter (PM_{2.5}): insights from the KORUS-AQ aircraft
720 campaign and seasonality, *Atmospheric Chemistry and Physics*, 1–23,
721 <https://doi.org/10.5194/acp-2021-413>, 2021.
- 722 Zhang, H., Hoff, R. M., and Engel-Cox, J. A.: The relation between moderate resolution imaging
723 spectroradiometer (MODIS) aerosol optical depth and PM_{2.5} over the United States: A
724 geographical comparison by U.S. Environmental Protection Agency regions, *Journal of the Air
725 and Waste Management Association*, 59, 1358–1369, [https://doi.org/10.3155/1047-
726 3289.59.11.1358](https://doi.org/10.3155/1047-3289.59.11.1358), 2009.
- 727 Zhang, L., Jacob, D. J., Knipping, E. M., Kumar, N., Munger, J. W., Carouge, C. C., Van
728 Donkelaar, A., Wang, Y. X., and Chen, D.: Nitrogen deposition to the United States: Distribution,
729 sources, and processes, *Atmospheric Chemistry and Physics*, 12, 4539–4554,
730 <https://doi.org/10.5194/ACP-12-4539-2012>, 2012.
- 731 Zhang, L., Kok, J. F., Henze, D. K., Li, Q., and Zhao, C.: Improving simulations of fine dust
732 surface concentrations over the western United States by optimizing the particle size distribution,
733 *Geophysical Research Letters*, 40, 3270–3275, <https://doi.org/10.1002/grl.50591>, 2013.
- 734 Zhao, B., Jiang, J. H., Diner, D. J., Su, H., Gu, Y., Liou, K.-N., Jiang, Z., Huang, L., Takano, Y.,
735 Fan, X., and Omar, A. H.: Intra-annual variations of regional aerosol optical depth, vertical
736 distribution, and particle types from multiple satellite and ground-based observational datasets,
737 *Atmospheric Chemistry and Physics*, 18, 11247–11260, [https://doi.org/10.5194/acp-18-11247-
738 2018](https://doi.org/10.5194/acp-18-11247-738), 2018.
- 739 Zhu, H., Martin, R. V., Croft, B., Zhai, S., Li, C., Bindle, L., Pierce, J. R., Chang, R. Y. W.,
740 Anderson, B. E., Ziemba, L. D., Hair, J. W., Ferrare, R. A., Hostetler, C. A., Singh, I., Chatterjee,
741 D., Jimenez, J. L., Campuzano-Jost, P., Nault, B. A., Dibb, J. E., Schwarz, J. S., and Weinheimer,
742 A.: Parameterization of size of organic and secondary inorganic aerosol for efficient representation
743 of global aerosol optical properties, *Atmospheric Chemistry and Physics*, 23, 5023–5042,
744 <https://doi.org/10.5194/ACP-23-5023-2023>, 2023.

745

746